Hindawi Publishing Corporation
Journal of Spectroscopy
Volume 2015, Article ID 826759, 12 pages
http://dx.doi.org/10.1155/2015/826759

Research Article

Corrosion Performance of AISI-309 Exposed to Molten Salts V_2O_5-Na_2SO_4 at 700°C Applying EIS and R_p Electrochemical Techniques

E. F. Diaz, C. Cuevas-Arteaga, N. Flores-García, S. Mejía Sintillo, and O. Sotelo-Mazón

Facultad de Ciencias Químicas e Ingeniería, Centro de Investigación en Ingeniería y Ciencias Aplicadas, UAEM, Avenida Universidad 1001, Colonia Chamilpa, 62209 Cuernavaca, MOR, Mexico

Correspondence should be addressed to C. Cuevas-Arteaga; ccuevas@uaem.mx

Received 11 February 2015; Revised 16 March 2015; Accepted 17 March 2015

Academic Editor: Djordje Mandrino

The corrosion performance of AISI-309 exposed 5 days to molten salts 50 mol% V_2O_5-50 mol% Na_2SO_4 at 700°C is reported in this paper. Such evaluation was made using three electrochemical techniques: potentiodynamic polarization curve (P_C), electrochemical impedance spectroscopy (EIS), and linear polarization resistance (R_p). From P_C, the Tafel slopes, I_{corr}, and E_{corr} were obtained. From Nyquist and Bode plots, it was possible to determine two different stages; the first one showed just one loop, which indicated the initial formation of Cr_2O_3 layer over the metallic surface; after that, the dissolution of Cr_2O_3 formed a porous layer, which became part of the corrosion products; at the same time a NiO layer combined with sulfur was forming, which was suggested as the second stage, represented by two capacitive loops. EIS plots were in agreement with the physical characterization made from SEM and EDS analyses. Fitting of EIS experimental data allowed us to propose two electrical circuits, being in concordance with the corrosion stages. Parameters obtained from the simulation of EIS data are also reported. From the results, it was stated that AISI-309 suffered intergranular corrosion due to the presence of sulfur, which diffused to the metallic surface through a porous Cr_2O_3 layer.

1. Introduction

Many industrial components operate at high temperatures, in which severe corrosion is found because of the aggressiveness of the environments. When the surface of a metal or alloy undergoes accelerated oxidation due to the presence of a thin film of high temperature molten salt, the formation of a crust of porous nonprotective oxide can be developed, so it is said that materials suffer a hot corrosion attack. In addition to the attack by reactive gases, materials used in these environments containing combustion products of fossil fuels are also attacked by salt deposits [1–3].

When using fossil fuels in energy generation systems, some chemical elements can form compounds with low melting points, which are called products of the combustion reactions. These compounds are deposited on the metal components of the system, and when the temperature is above its melting point, they can generate catastrophic corrosion phenomenon [4]. The hot corrosion phenomenon has been investigated since early 1940 in boilers and their components, internal combustion engines, gas turbines, and incinerators. However, this issue gained importance and interest until 1960, when gas turbine engines for military aircraft in the Vietnam conflict suffered a severe corrosion [5].

Combustion processes produce ashes, which have a high concentration of vanadium and sodium sulfate, from which some other more corrosive mixtures are usually formed [6]. Among the compounds formed from the primary elements such as S, Na, and V, many have melting points below 600°C. These low melting points compounds can contribute to the formation of very sticky molten deposits, allowing greater diffusion rates of harmful elements, which cause accelerated attack [7]. Many components of gas turbines, boilers, and equipment that produce energy are made of stainless steel materials; however, stainless steel 309 has been poorly studied in environments containing V_2O_5-Na_2SO_4. Stainless steels are considered highly resistant to corrosion in oxidizing atmospheres at temperatures up to 1100°C. Due to its high

chromium content of 25–28%, these alloys typically form and maintain slow growing protective scales of Cr_2O_3 [8, 9]. Gao et al. [10] reported that many high-temperature alloys are susceptible to hot corrosion, which makes the selection of materials difficult; however, an increase in the chromium content can be beneficial. According to Singh et al. [9], the resistance of stainless steels to high temperature primarily arises from the formation of protective chromia (Cr_2O_3), which protects the underlying metal from further oxidation. However, the presence of molten salt deposits can lead to accelerated oxidation and hot corrosion, whose corrosion products comprise internal oxides and sulfides; therefore, under these conditions a rapid material degradation is observed.

Wu et al. [3] have reported that the corrosion of metals in molten salts can be explained by the combination of the anodic oxidation of metals and cathodic reduction of the oxidants such as in aqueous electrolytes systems. This phenomenon is caused by the oxidation of the elements forming the alloys, the reduction of oxidant species, and then the formation of compact or porous corrosion films and their fluxing by molten salt mixtures [11]. Due to the difficulty to determine the corrosion rate of metals and alloys in molten salts when the Tafel region of the polarization curves is very limited, the linear polarization resistance technique (R_p) has been reported to correlate well with the results obtained from the weight loss method [6, 12, 13]. However, many high temperature corrosion studies have been carried out to determine corrosion rates of alloys exposed to Na_2SO_4-V_2O_5 mixtures with different concentrations using different electrochemical techniques, such as electrochemical impedance spectroscopy and electrochemical noise [6, 14–16].

In this paper, AISI-309 was studied in molten salt with a composition of 50 mol% V_2O_5-50 mol% Na_2SO_4 exposed at 700°C for 5 days, applying three electrochemical techniques: potentiodynamic polarization curve, electrochemical impedance spectroscopy, and linear polarization resistance. In order to determine the type of corrosion suffered by the alloy after exposure for 5 days, the physical characterization of the corroded samples and EDS analysis of the corrosion products were made through SEM.

2. Materials and Methods

The chemical composition of AISI-309 is shown in Table 1, which was obtained from the supplier (Sandmeyer Steel Company, Philadelphia, PA, USA) through the certification of the chemical analysis authenticity.

The molten salt was prepared with analytical reagents: 50 mol% V_2O_5-50 mol% Na_2SO_4 and the test temperature was 700°C. The amount of molten salt used for the three techniques in each experiment was 500 mg/cm^2. Molten salt corrosion where Na_2SO_4-V_2O_5 mixtures are present has been studied for several decades. Some authors [17, 18] performed experiments with different stainless steels in presence of diverse compositions of Na_2SO_4-V_2O_5 molten salts in static air, in a range of temperatures of 610–900°C. These authors concluded that none of these materials were satisfactorily resistant and that the most severe corrosion was presented when the salts contained from 10 to 30 mol% of Na_2SO_4 and the rest of V_2O_5, observing the maximum corrosion at 20 mol% Na_2SO_4-80 mol% V_2O_5 at temperatures higher than 760°C. At temperatures lower than 760°C, this behavior was different, observing an almost constant corrosion rate along all the compositions, which were from 0 to 100 mol% of Na_2SO_4 and V_2O_5. Given that hot corrosion is mainly seen in superheaters and reheaters of boilers, gas turbines, and furnaces, whose temperatures are between 600 and 700°C, in the present study, one of the aims was to determine the corrosion performance of AISI-309 with a high content of chromium of 22.2% (many commercial stainless steels have less than 20% of chromium). Fuel ash corrosion is mainly presented when the formation of mixtures derives from the primary compounds such as Na_2SO_4 and V_2O_5, and depending on the composition of S, V, and Na in the fuel oil, diverse compositions of these mixtures can be formed. Therefore, the present research is a contribution in the study of high temperature corrosion of the AISI-309 under the experimental conditions stated in this paper.

Table 1: Chemical composition (wt.%) of AISI-309.

Si	P	S	Cr	Mn	Fe	Ni	C
0.41	0.023	0.004	22.2	1.78	60.8	14.71	0.035

On the other hand, along many hot corrosion studies utilizing Na_2SO_4-V_2O_5 molten salts, it has been possible to state two corrosion mechanisms [19]: accelerated oxidation due to the dissolution of the oxide layers formed over the metallic surfaces due to the presence of V_2O_5 and sulfidation followed by oxidation due to the presence of Na_2SO_4. When vanadium is present in high composition, the first mechanism is expected, whereas when sulfur is present in high composition, the second mechanism will predominate. In such cases where the composition of both compounds is similar (such as the present study) both mechanisms can contribute in some way.

Samples were cut 7 × 6 × 6 mm, metallographically prepared starting with SiC grit with a grain size of 120, 480, and 600. Each sample was welded on one of its sides to nicromel wire (20Cr-80Ni), washed in distilled water, degreased with acetone, and dried under an air stream. Once welded samples were ready, the 80Ni-20Cr wire was introduced inside a ceramic tube with dimensions of 8.0 mm of inner diameter and 200 mm of length. The gap between the wire and the ceramic walls was sealed with refractory cement. The electrochemical cell was constituted by the working electrode (AISI-309) and two platinum wires as reference and auxiliary electrodes, which were also prepared following the same procedure as that for the working electrode.

This electrochemical cell was introduced inside the electrical furnace in a 20 mL ceramic crucible containing the corrosive mixture, which was melted when the electrical furnace reached a temperature of 700°C ± 2°C, which was kept during the test period. The temperature of the furnace

was monitored by a K type thermocouple, which in turn was connected to an analogical multimeter. The ceramic crucible together with the solid corrosive salt was replaced for each experiment. The experimental procedure carried out in this work was deep melt tests in static air; therefore the experimental conditions are not representative of fireside corrosion conditions; however, bulk molten salt tests are a viable proposition for material corrosion evaluation.

2.1. Procedure for P_C Electrochemical Tests. To perform the potentiodynamic polarization curve (P_C), linear polarization resistance (R_p), and the electrochemical impedance spectroscopy (EIS), a set of three electrodes was used, as was explained before. The two platinum wires as reference and auxiliary electrodes have been used very frequently [14–16]. Before exposing the samples, the area in contact with the molten salt was determined.

For data collection, the electrodes were connected to an AC Gill potentiostat automated connected via an interface to a personal computer. Polarization curve were obtained 30 minutes after exposing the specimen to the corrosion mixture, which was when the corrosion potential reached a stable condition. For the polarization curve, overpotential of −300 to 1000 mV was applied with a scan rate of 1 mV/s. When the test temperature was stabilized, the three-electrode cell was introduced inside the molten salt and the connection between the electrodes with the potentiostat was made immediately. The Tafel slopes (b_a, b_c) were established from the active regions of the polarization curve of the corresponding anodic and cathodic branches.

2.2. Procedure for R_p and EIS Tests. To determine R_p data, a linear polarization of ±10 mV was applied with respect to the corrosion potential at a scan rate of 1 mV/s. The R_p tests were carried out following the procedure according to ASTM G 59 standard [20].

EIS technique was performed in order to determine the corrosion mechanism according to the Nyquist and Bode plots and their fitting to electrical circuits, both taking into account the physical characterization of the corroded samples. The frequency range selected for EIS was from 10 kHz to 1 mHz. The wave-signal amplitude was of 10 mV. R_p and EIS were applied for 5 days of exposure.

The corroded samples from EIS and R_p were analyzed by SEM after 5 days of exposure. Before SEM analyses and in order to determine the type of corrosion suffered by AISI-309 exposed to the molten salt, the corroded sample from R_p was mechanically clean for taking out the corrosion products, whereas the corroded sample from EIS was mounted (without descaling) in bakelite, metallographically polished, and the cross section was analyzed to investigate the morphology and distribution of reaction products. Through SEM analysis, an electron image of the metal-scale interface and X-ray mappings of the mean elements of the corroded system were obtained. Also, some EDS analyses of some traces of corrosion products adhered to the metallic surface were obtained from R_p corroded samples.

3. Results and Discussion

3.1. Physical Characterization. Figure 1 shows the SEM image of AISI-309 after the corrosion tests in 50 mol% V_2O_5-50 mol% Na_2SO_4 at 700°C and the corresponding X-ray mappings of elements O, Cr, Ni, Fe, S, Na and V. As it is shown, the micrograph provides an interface between the metal surface and the corrosion products over the surface. Mappings show that the scale has a low-medium concentration of chromium and iron, which are related to oxygen. It seems to be that, after 5 days of exposure, the initially formed chromium and iron oxides have been dissolved by effect of the molten salt species, allowing the diffusion of aggressive species to the surface alloy, since the mapping of sulfur shows a thin layer of sulfur just in the metal-scale interface, below the chromium and iron layers. Nevertheless, a 5 μm thick oxygen layer is noted below the sulfur layer, maybe related to nickel, since the empty space presented by Cr and Fe is not evident in the mapping of nickel, so the layer of oxygen must be related to nickel, as it has been presented in some other V_2O_5-Na_2SO_4 systems at high temperature [14]. From the above observations, it can be inferred that, during the corrosion process, some chromium mass loss was presented in the matrix by the effect of the oxidation reactions. Afterward such chromium was transformed into a passive layer of Cr_2O_3 as a reaction of the alloy to be protected, and then this initially dense and coherent passive layer of chromium oxide was evenly dispersed with a trend to be dissolved, as it can be seen in the corresponding mapping. It is possible that the place initially occupied by the chromium inside the alloy has been replaced by nickel, which has probably diffused from the matrix to the metal-oxide interface enhancing the alloy surface of nickel. The chromium oxide is one of the most protective compounds when molten salts are present [3, 6].

On the other hand, as mentioned by Gao and Li [21], the deficiency of oxide ions in the process through which the corrosion products fail to be protective is due to the formation of species that are soluble in the fluid reservoir, which leads to "fluxing" reactions. The fluxing reactions provoke the fact that corrosion products formed during the exposure to the molten salts do not be protective anymore, which is evident in the chromium and iron mappings, observing a porous layer through which the corrosive species could diffuse to reach the metallic surface, such as sulfur.

Rapp et al. [2] also suggest that the oxide scales normally should form a protective barrier on the surface of the alloy, but oxide such as Cr_2O_3 is soluble in molten salt containing vanadium, sulfur, and sodium, since it forms chromate ions or vanadate compounds, inducing the initially protective layer to become porous. On the other hand, Tzvetkoff and Kolchakov [11] mention that the Cr_2O_3 layer formed on the gas turbines is very stable in molten sulphates because the pO^{-2} of the molten sulphates minimizes their solubility. Nevertheless, the results of the present study show that the addition of vanadium in molten salt increases the corrosiveness of the molten salt becoming the initially protective Cr_2O_3 layer in a porous one.

Figure 2 shows two micrographs at different magnifications of AISI-309 exposed to 50 mol% V_2O_5-50 mol%

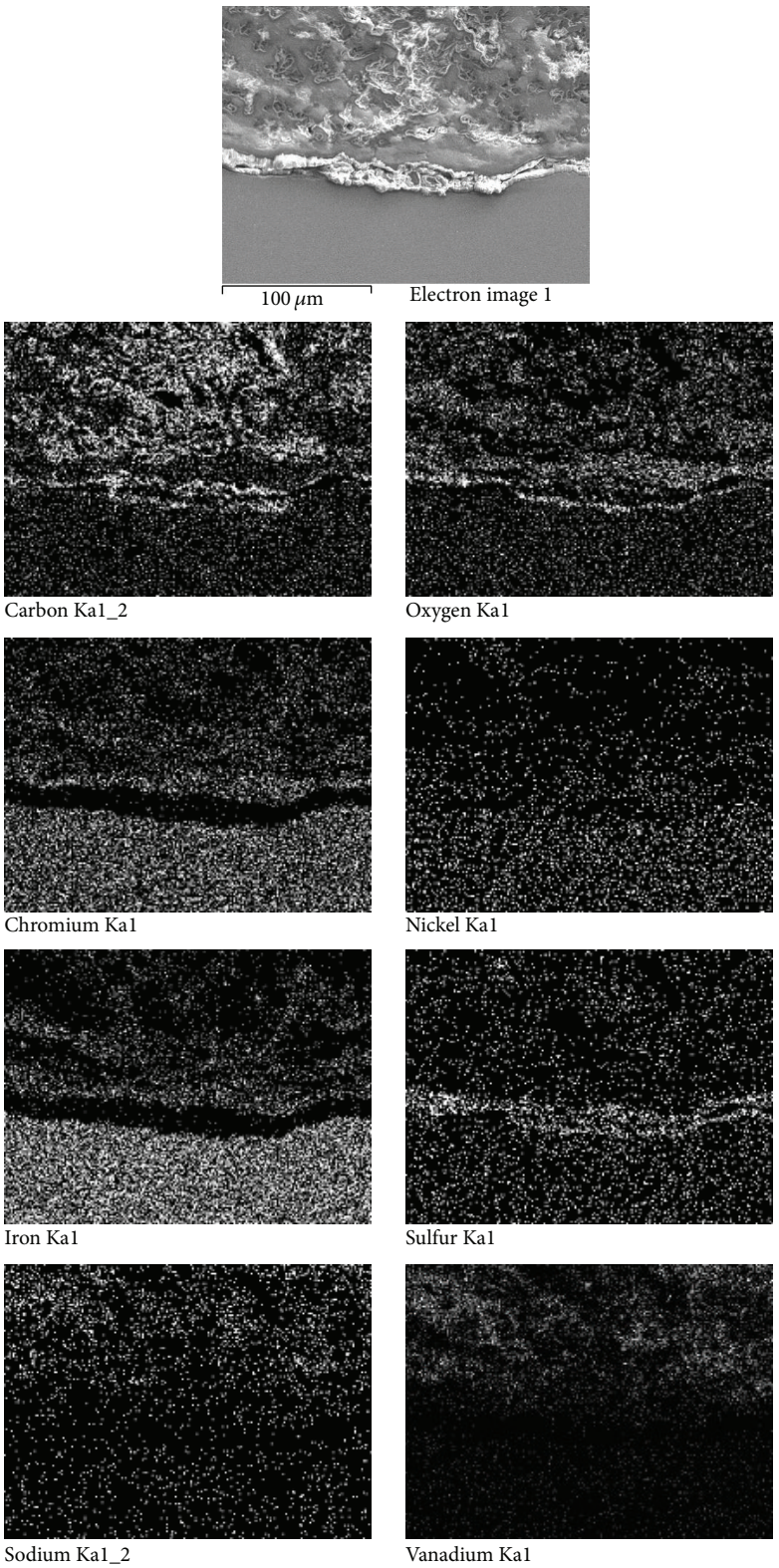

Figure 1: Energy dispersive X-ray maps of cross sections of stainless steel 309 after immersion tests in 50 mol% V_2O_5-50 mol% Na_2SO_4 at 700°C.

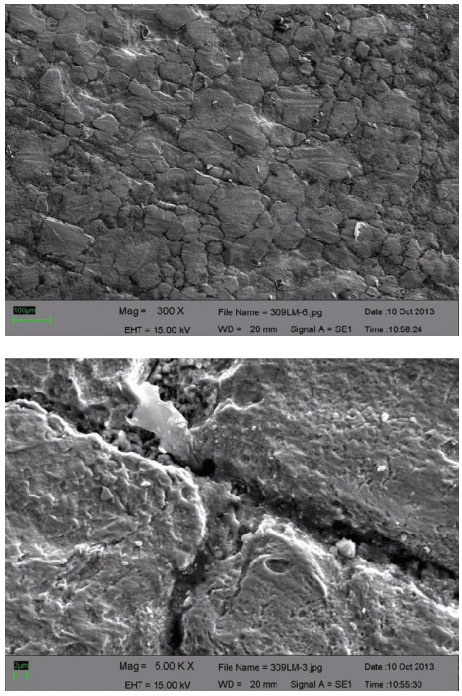

Figure 2: Micrographs of AISI-309 after five days of exposure in molten salts 50 mol% V_2O_5-50% Na_2SO_4 at 700°C.

Na_2SO_4 mixture for 5 days at 700°C obtained after using the R_p technique. The images evidence an intergranular corrosion process over the entire surface, clearly showing the revealed grain boundaries. The shape of the grains is irregular, and their sizes lie between 20 μm and 200 μm. Some traces of corrosion products are present in the grain boundaries, but also there are hollows in some of these zones. In some regions, corrosion products can be seen outside the grain boundaries covering partially the core of grains. Also, a great amount of pores can be seen and this porosity indicates the selective oxidation of some alloying element of the material. From the Cr and Fe mapping, it seems that these alloying elements were those suffering selective oxidation from the beginning of the corrosion process.

Figure 3 shows two EDS analyses made to some adhered traces of the corrosion products of the cleaned corroded sample presented in Figure 2. These EDS analyses show the presence of the main elements of the alloy such as chromium, iron, and nickel. Silicon and manganese were presented too, although such result was not evident from the mappings, which was probably due to their low concentration of these elements in the alloy. The presence of oxygen in both EDS results shows the probable oxidation of these five elements and the subsequent formation of their corresponding oxides. EDS analyses also presented sulfur, whereby it is confirmed that, after five days of exposure, the oxide layers became porous and not protective, so that some corrosive species such as sulfur could diffuse not only to reach the metallic surface but also to penetrate to the matrix of the alloy and produce the intergranular corrosion process, probably through sulfidation, according to the mapping of sulfur.

Table 2: Electrochemical parameters obtained from polarization curve for stainless steel 309 in molten salts 50 mol% V_2O_5-50 mol% Na_2SO_4 at 700°C.

E_{corr} (mV)	I_{corr} (mA/cm^2)	b_a (mV/dec)	b_c (mV/dec)	R_p (ohms·cm^2)
−7.66	9.2168	297.75	246.04	6.34

3.2. Potentiodynamic Polarization Curve. Figure 4 shows the polarization curve obtained for stainless steel 309 in molten salts 50 mol% V_2O_5-50 mol% Na_2SO_4 at 700°C. It can be seen that the shape of the curve shows only an active-transactive behavior, without the formation of a passive layer, showing that the formation of corrosion products may be only partially protective, which is in accordance with the physical characterization, in which it was observed that corrosion products, especially chromium and iron oxides, became porous. Anodic polarization may sometimes produce concentration effects, due to passivation and dissolution, as well as roughening of the surface, which can lead to deviations from Tafel behavior.

It is also seen that the cathodic and anodic branches of the polarization curve display a not typical Tafel behavior, since the magnitudes of the Tafel slopes are bigger than 100 mv/dec. Skinner [22] has indicated that slopes higher than 100–120 mV/dec are common for those systems having important diffusion phenomena. It is possible that the diffusion of sulfur to the metallic surface, through the porous chromium-iron layers, is one of the diffusion processes taking place during the corrosion phenomenon [23], which would explain the presence of sulfur in the metallic scale.

Table 2 shows the parameters obtained from Tafel extrapolation method; the polarization resistance R_p was calculated using the Stern-Geary equation [24–26]. R_p value resulted from 6.34 ohms·cm^2, which seems to be very small, evidencing that AISI-309 does not protect itself against sodium sulphate/vanadium oxide molten salt at 700°C, which is in accordance with the corrosion rate obtained from the electrochemical noise technique and the conventional weight loss method reported elsewhere [15]. Consider

$$I_{corr} = \frac{B}{Lpr}$$
$$B = \frac{b_a b_c}{2.303\ (b_a + b_c)}. \quad (1)$$

Wu et al. [3] reported that a protective film of Cr_2O_3 may be formed on the surface of the working electrode when the chromium content is greater than 20 wt.%. However, as shown in Figure 4, the anodic curve did not present a passivation behavior at the potential range of the curve, such that it was deduced before through the physical evidences. It is possible that a chromium oxide layer had been formed at the beginning of the corrosion process, dissolving it afterward in time until becoming in a porous layer (see Cr mapping). These results are in agreement with those obtained from EIS technique, which will be presented in Table 2.

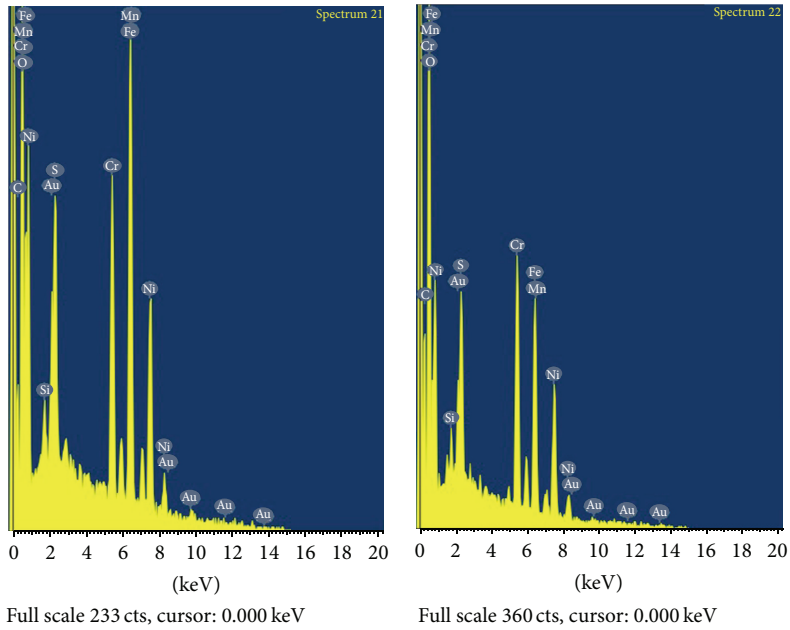

Figure 3: EDS analyses of corrosion products of AISI-309 after five days of exposure in molten salts 50 mol% V_2O_5-50 mol% Na_2SO_4 at 700°C.

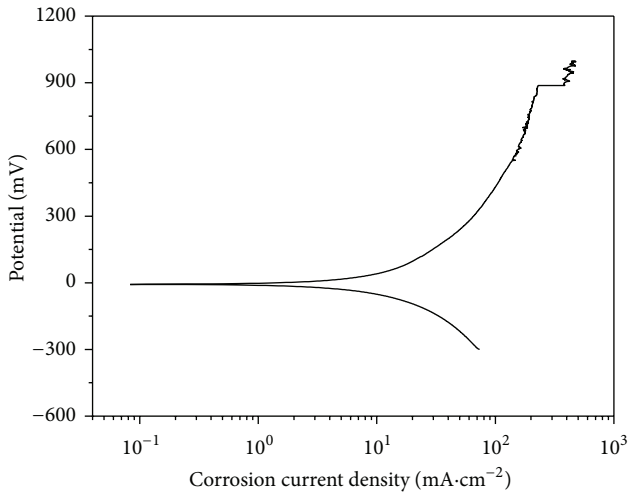

Figure 4: Polarization curve for AISI-309 exposed to 50 mol% V_2O_5-50 mol% Na_2SO_4 at 700°C.

3.3. Electrochemical Impedance Spectroscopy. Figure 5(a) shows three Nyquist plots for AISI-309 obtained at the beginning, 20 hours, and 40 hours, while Figure 5(b) shows the Nyquist plots at 50, 70, 90, 100, and 120 hours obtained during the 5 days of exposure in molten 50 mol% V_2O_5-50 mol% Na_2SO_4 at 700°C. Nyquist plots show that, during the first 40 h of immersion, the impedance spectrum is composed just for one capacitive loop at high frequency, whose charge transfer resistances were in a range of 13.67 to 19.15 ohms·cm^2. EIS diagrams are not perfect semicircles, having the center under the real axis. This behavior is characteristic for solid electrodes and usually referred to frequency dispersion which has been attributed to the heterogeneities of the metal surfaces and mass transport processes [27]. The presence of one just semicircle implies the presence of one singular oxide layer at the beginning of the corrosion process [28]. Considering the physical characterization, it is possible that this oxide layer had been formed by Cr_2O_3. It has been stated that when an alloy exceeds the 20% of its chromium content, the corrosion resistance improves significantly [3]. Chromium oxide is considered the main element to protect against molten salt corrosion, especially the austenitic stainless steels, which also contain nickel, forming a chromium oxide at the beginning of the corrosion process, which starts to dissolve and become porous in time; after that the formation of a nickel oxide below the Cr_2O_3 layer is common [6, 14, 15], as was observed in the present case. Taking into account the results from the mapping of chromium, it is possible to say that chromium oxide was protective at the beginning of the exposition of AISI-309 to sodium sulfate-vanadium oxide molten salt, when the diffusion of sulfur from the molten salt layer was not still so evident. The alloys used in high temperature corrosion by molten salts normally obtain their protection from a dense, adherent, and coherent metallic oxide of slow growth; nevertheless when the material is covered by a light molten salt deposit, the protective metallic oxide can be penetrated by aggressive species such as sulfur, oxygen, or even vanadium; then the oxidation rate is accelerated and materials can suffer internal degradation or in some cases catastrophic effects, presenting small charge transfer resistances.

After 50 h immersion a second capacitive loop was formed, a very small depressed semicircle at high frequency and a larger depressed semicircle at low frequency, which show two time constants, as has been reported by Tan et al.

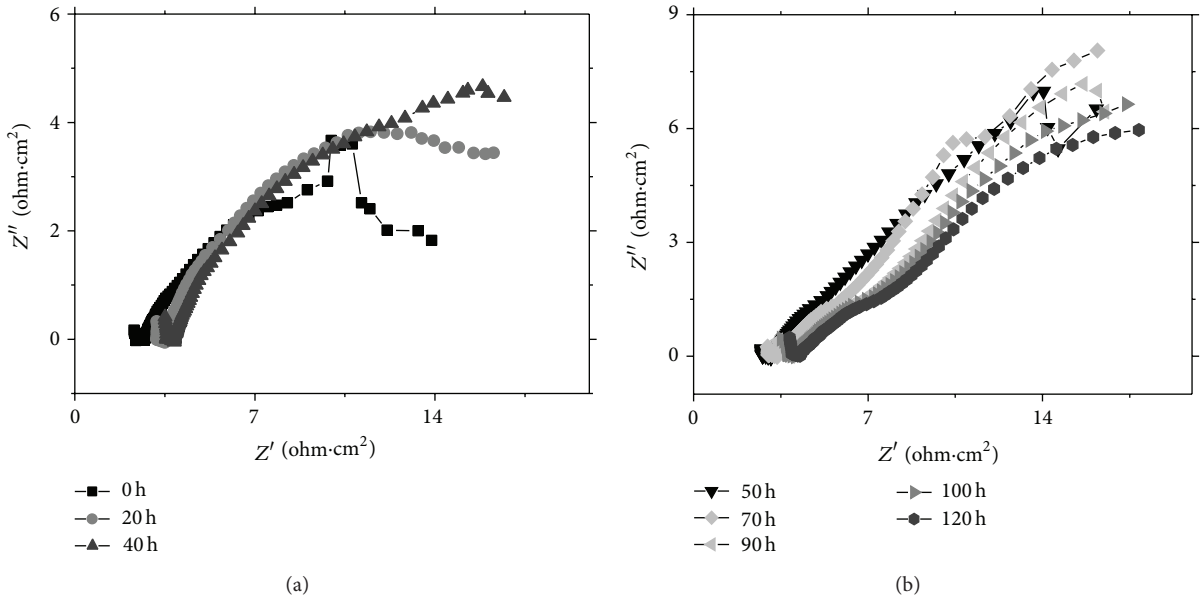

FIGURE 5: Nyquist plots for stainless steel 309 exposed to molten salts 50 mol% V_2O_5-50 mol% Na_2SO_4 at 700°C.

[29]. Two semicircles indicate the possible formation of two layers. According to the mappings presented in Figure 1, one of the layers can be attributed to the corrosion products near or in combination with the molten salts, and the other one is presented near the metallic surface, which could be a chromium oxide (still protective) or a nickel oxide related to sulfur at the last hours of the exposure. The outer layer seems to be formed by porous chromium and iron oxides together with vanadium, sulfur, and sodium. The formation of a porous layer indicates the dissolution of Cr and Fe due to the presence of vanadium, possibly in the form of chromium and iron vanadates, as has been reported under similar conditions of exposure of alloys containing Cr, Fe, and Ni [6, 15, 16]. The inner layer, present in the scale/alloy interface, was composed initially by a chromium oxide layer and once this layer became porous due to dissolution, porous Cr_2O_3 formed part of the corrosion products layer and a nickel related to sulfur was formed, as has been reported elsewhere [15, 16, 30, 31].

Figure 6 presents the experimental and fitted Nyquist and Bode plots of EIS results at 20 and 120 hours for stainless steel 309 exposed to molten salts 50 mol% V_2O_5-50 mol% Na_2SO_4 at 700°C as an example of the two different behaviors encountered along the exposure time, whereas Figures 7(a) and 7(b) present the Bode plots of the experimental data corresponding to the Nyquist plots presented in Figure 5. From Figure 6, the upper plots correspond to the first behavior from the beginning to 40 hours, showing one single capacitive loop, and the lower plots correspond to the behavior obtained from 50 to 120 h, showing two capacitive loops. From both scenarios, it is possible to observe a good concordance from the experimental and fitted data, observing the presence of just one time constant in Bode plots for the results until 40 hours and two time constants for the results from 50 hours to the end of the experiment. The fitting of the experimental data allows us to propose two electrical circuits, which are presented in Figure 8.

For the results at the beginning, 20 hours, and 40 hours, a simple Randles circuit was proposed (Figure 8(a)) [32–34]. This circuit is the simplest in order to identify a corrosion process, where a corrosion mechanism can be fitted as an equivalent circuit of three elements: the electrolyte/metal interface represented by a resistor R_{ct} (charge transfer resistance) in parallel with a capacitor C_{dl} (double electrochemical layer) and the electrolyte resistance (R_s) represented by a second resistor in series with the interface [35]. The charge transfer resistance corresponds to the corrosion reaction at metal substrate/solution interface, whose value is a measure of electron transfer across the surface and is inversely proportional to corrosion rate. Some authors [36, 37] have indicated that the criterion in the election of an electrical equivalent circuit in order to fit the electrochemical impedance data is taking into account a resume of the Bode diagrams (impedance module and phase angle). It is evident that the physical characterization results and its interpretation accordingly with the corrosion phenomenon must be also in accordance with the equivalent circuit. For the results from 50 to 120 hours, the impedance model was fitted to two loops representing the impedance responses from the double-layer capacitance at low frequency in parallel with the oxide capacitance at high frequency (Figure 8(b)). The electrolyte resistance is in series with these two elements.

It is known that in systems containing oxide metallic layers (corrosion studies) the measurement of the capacitive response is not ideal, which means that it is not possible to talk about a pure capacitor. Due to this deviation and in order to get a more accurate fitting of the experimental electrochemical impedance data, a constant phase element

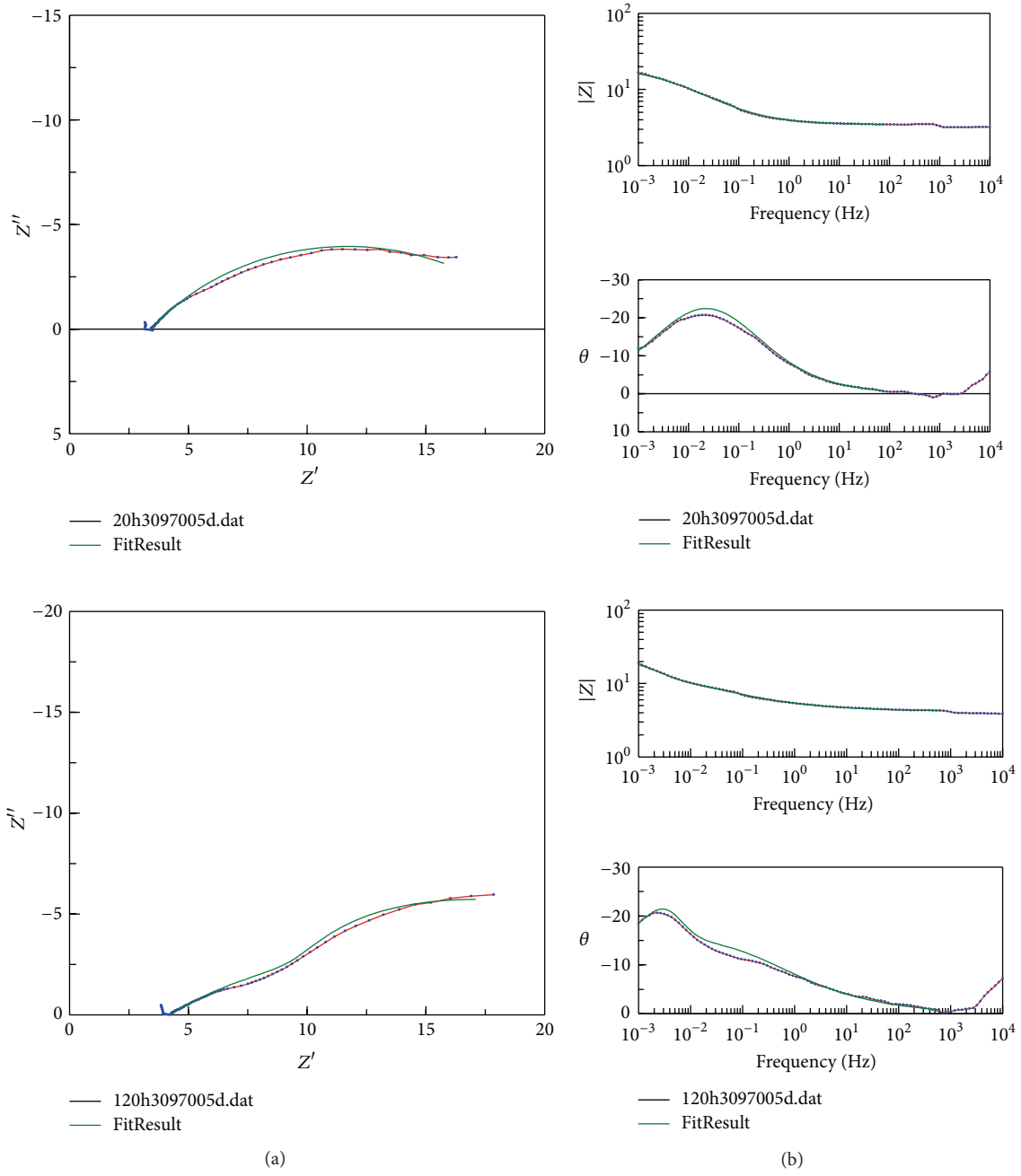

FIGURE 6: Experimental (red with blue circles) and fitted (green solid line) Nyquist (a) and Bode (b) plots obtained for stainless steel 309 exposed to molten salts 50 mol% V_2O_5-50 mol% Na_2SO_4 at 700°C.

(CPE) has been used instead of an ideal capacitive element [38, 39]. Therefore, the impedance that best represents a CPE is given by the next correlation:

$$\mathrm{ZCPE} = Y_0^{-1} (j\omega)^{-n}, \quad (2)$$

where ZCPE represents the impedance of CPE, Y_0 is the pseudocapacitance or a proportionality coefficient, j is the imaginary number, ω is the angular frequency, and n is an exponent related to the phase shift, and it can be used as a measure of surface irregularities and also associated with the nonuniform distribution of current as a result of roughness and surface defects [40]. "n" is also called phenomenological coefficient. In an ideal case when the exponential factor "n" is equal to 1 ($n = 1$), the CPE behaves as an ideal capacitor, and Y_0 is equal to the capacitance "C." In real systems (as corrosion systems), when $0.5 < n < 1$, the system is not ideal anymore; therefore, the adjustment must be made for both "C" and "n." In general, a constant phase element (CPE) is used instead of a pure capacitor to compensate for nonideal capacitive response of the interface [41, 42], which is related to heterogeneities of the metallic surface or in the metallic

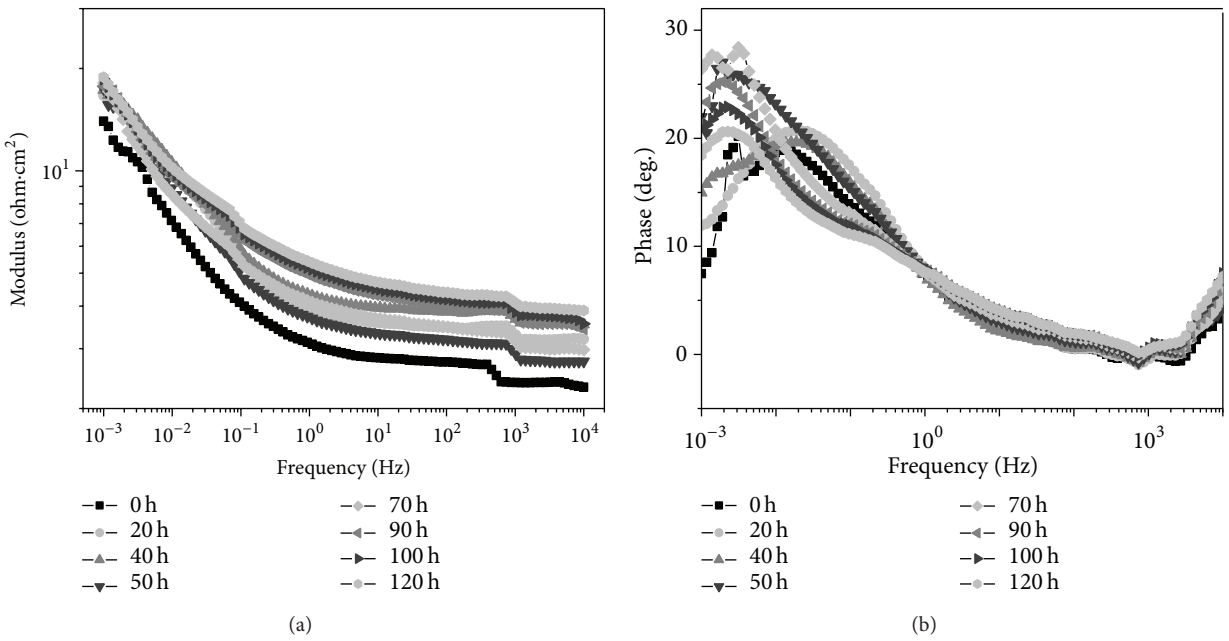

Figure 7: Bode plots for stainless steel 309 exposed to molten salts 50 mol% V_2O_5-50 mol% Na_2SO_4 at 700°C.

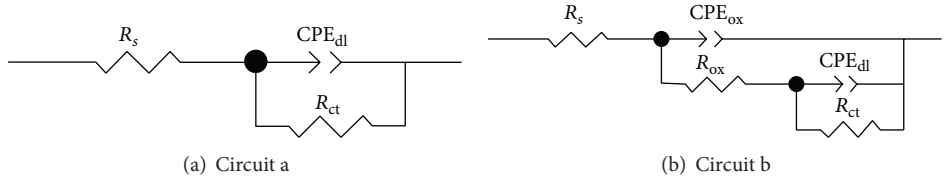

Figure 8: Electrical circuits used to simulate the EIS data for AISI-309 in molten salts 50 mol% V_2O_5-50 mol% Na_2SO_4 at 700°C.

oxide layer, as was said before. The fitted results are given in Table 3.

At the beginning, 20 hours, and 40 hours, the charge transfer resistance R_{ct} corresponds to the response of AISI-309, in whose surface a chromium oxide layer was formed due to the exposure of the molten salt. Due to R_{ct} increasing at this first stage, it is possible to say that Cr_2O_3 was a good protective layer until 40 hours. After that, from 50 to the end of the test, it is possible to expect that, until 70 hours, when R_{ct} is still increased, the presence of a chromium oxide layer keeps over the metallic substrate, but at the same time the dissolution of this layer far away from the metal/oxide layer interface and close to the oxide layer/molten salts is carried out, keeping its protectiveness near the metallic surface; that is why the R_{ct} is increased from 19.15 ohms·cm^2 to 89.57 ohms·cm^2. At the same time, the resistance (R_{ox}) of the second layer (corrosion products, outer layer) has a small value due to the almost only existence of molten salts (whose value is very close to the solution resistance R_s, being of 3.39 ohms·cm^2 compared to that of R_s, which is 3.0 ohms·cm^2). At 70 hours, R_{ox} increased, presumably due to the major presence of porous chromium oxide in the corrosion products. After that, R_{ox} was decreasing to values close to that of R_s, whose value corresponds to the corrosion products layer formed by the dissolved metallic oxides (Cr and Fe) together with an important amount of corrosive species such as vanadium, sodium, and sulfur. The values of R_{ct} after 70 hours decreased significantly, which was due to the fact the chromium oxide had become porous and had diffused to the outer layer (corrosion products); therefore, R_{ct} would now correspond to the nickel oxide-sulfur layer, whose values of R_{ct} are between 22.80 and 30.62 ohms·cm^2. The value of R_s is lightly increased in time, which is due to the changes suffered by the molten salts when metallic oxides are diffused and mixed with the molten salts, probably forming species such as metallic vanadates, sulfurs, or sulfates, which were evident with the physical observations from the mappings obtained from SEM and EDS analysis. It may also be noted that the values of n_{dl} as n_{ox} are not approaching unity; this is consistent with that reported in the literature regarding the effect of dispersion that occurs in high temperature corrosion in molten salts [43].

All values of n_{dl}, except that at 50 h (whose value is 0.9), deviate from 1, indicating a strong dispersion effect, which is common in molten salt corrosion, and it is associated with roughness and surface defects. Values of n_{ox} are smaller than 0.5, indicating that this corrosion system is highly resistive, referring to the corrosion products containing a great amount

Table 3: Calculated parameters obtained from the simulation of EIS experimental data for AISI-309 exposed in molten salts 50 mol% V_2O_5-50 mol% Na_2SO_4 at 700°C.

Time (h)	R_s (ohms·cm^2)	CPE_{ox} (μF/cm^2)	n_{ox}	R_{ox} (ohms·cm^2)	CPE_{dl} (μF/cm^2)	n_{dl}	R_{ct} (ohms·cm^2)
0	2.7	—	—	—	0.697	0.56	13.67
20	3.4	—	—	—	0.444	0.56	16.53
40	3.8	—	—	—	0.447	0.54	19.15
50	3.0	0.498	0.43	3.39	0.034	0.90	58.07
70	3.3	0.477	0.41	16.62	0.357	0.79	89.57
90	4.0	0.432	0.47	12.58	0.696	0.65	28.07
100	4.0	0.266	0.48	6.36	0.889	0.60	30.62
120	4.2	0.265	0.45	7.30	0.908	0.64	22.80

of molten salts. The capacitance of the double electrochemical layer CPE_{dl} of the substrate, which was in contact initially with the chromium oxide and then with the nickel oxide related to sulfur, is in general increasing, which means that the oxide layer is decreasing, as was shown in the maps of chromium, indicating the instability of the passive layer and its porosity; that is why the corrosive species diffused to the metallic surface provoking intergranular corrosion, as was observed from the corroded samples in Figure 2.

Figure 9 shows a comparison of R_p and R_{ct} when AISI-309 was exposed to 50 mol% V_2O_5-50 mol% Na_2SO_4 at 700°C. R_p values resulted smaller than R_{ct}, which is not an expected result, since R_p is the sum of R_{ct} plus R_s; nevertheless the results from both techniques are in the same order of magnitude. The behavior of both plots is similar from the beginning until 70 hours, where the corrosion resistance is increasing; after that data from R_{ct} indicates that the corrosion resistance decreases until the end of the exposure time, which is in congruence with the physical observations from SEM images. It is expected that, after the complete dissolution of Cr_2O_3 and the formation of NiO mixed with sulfur, the layer over the metallic surface is not protective, producing a localized attack as intergranular corrosion, and therefore the corrosion resistance would decrease, such as the behavior showed from R_{ct} values. In the case of R_p, its behavior shows a continuous increase until the end of the exposure. The results obtained from the EIS technique are in agreement with previous reported results of AISI-309 studied under the same conditions but obtained from the electrochemical potential and current noise technique, from which the noise resistance was determined together with the weight loss method [15]. From the present results and that previously reported, it is possible to say that linear polarization resistance technique did not present consistency in its results with respect to the corrosion performance of AISI-309 evidenced from physical characterization.

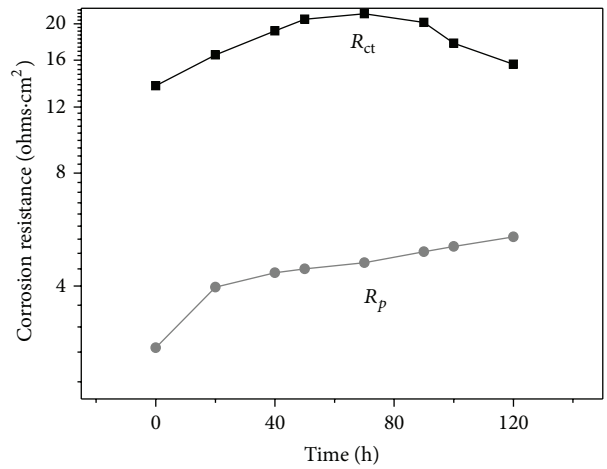

Figure 9: Values of R_p and R_{ct} values obtained from R_p and EIS techniques.

4. Conclusions

A study of corrosion performance from the EIS and R_p together with SEM and EDS analysis was obtained for the stainless steel AISI-309 exposed for 5 days to 50 mol% V_2O_5–50 mol% Na_2SO_4 molten salt at 700°C. The results indicated that AISI-309 presented a major dissolution of the initially chromium and iron oxides layers formed during the first corrosion stage, after which a medium concentrated nickel oxide layer was observed in combination with sulfur. The optical images of AISI-309 free of corrosion products together with the SEM mappings of the main elements of the corrosive system and EDS analysis supported these conclusions.

From EIS results, it was possible to determine two different behaviors from Nyquist and Bode plots; the first one showed just one loop, which indicated the initial formation of a chromium oxide layer over the metallic surface (first corrosion stage); after that, the dissolution of Cr_2O_3 forming a porous layer in parallel with the formation of a second nickel oxide layer combined with sulfur was suggested as the second stage, which was in agreement with the physical characterization made from SEM and EDS observations. The second stage consisted in the development of a corrosion products layer formed of porous Cr_2O_3, in which interstices molten salt was introduced, and the presence of a NiO-S layer in contact with the substrate. Fitting of EIS experimental data allowed us to propose two electrical circuits, which were in concordance with the two corrosion stages. Calculated parameters obtained from the simulation of experimental

EIS data were reported and analyzed. The behavior of R_{ct} together with SEM images and EDS analyses showed that AISI-309 suffered intergranular corrosion due to the presence of the aggressive species sulfur, which diffused to the metallic surface.

From the present results and that previously reported [15], it is possible to say that linear polarization resistance technique did not present concordance with respect to the corrosion performance of AISI-309 evidenced from physical characterization and the EIS technique.

Conflict of Interests

The authors declare that there is no conflict of interests regarding the publication of this paper.

Acknowledgments

The first author gratefully thanks CONACYT for the postdoctoral scholarship, under Reference no. 290805, who was under the supervision of C. Cuevas-Arteaga. In addition, the authors would like to thank Rene Guardian Tapia from CIICAP-UAEM for his support to carry out SEM studies.

References

[1] N. Birks, G. H. Meier, and F. S. Pettit, *Introduction to the High-Temperature Oxidation of Metals*, Cambridge University Press, Cambridge, UK, 2nd edition, 2006.

[2] R. A. Rapp, J. H. Devan, D. L. Douglass, P. C. Nordine, F. S. Pettit, and D. P. Whittle, "High temperature corrosion in energy systems," *Materials Science and Engineering*, vol. 50, no. 1, pp. 1–17, 1981.

[3] C. X. Wu, A. Nishikata, and T. Tsuru, "AC Impedance and electrochemical techniques for evaluating hot corrosion resistance," in *High Temperature Corrosion of Advanced Materials and Protective Coatings*, pp. 221–225, Elsevier Science Publishers, 1992.

[4] E. Otero, A. Pardo, F. J. Pérez, J. F. Álvarez, and M. V. Utrilla, "A high temperature corrosion kinetic study of HK-40 superalloy surface treated, in contact with eutectic mixture 82%$K_2S_2O_7$-18%V_2O_5," *Corrosion Science*, vol. 39, no. 1, pp. 133–145, 1997.

[5] M. Schütze, "Corrosion resistance at elevated temperatures in highly aggressive environments," *Corrosion*, vol. 63, no. 1, pp. 4–18, 2007.

[6] C. Cuevas-Arteaga, J. Uruchurtu-Chavarín, J. Porcayo-Calderon, G. Izquierdo-Montalvo, and J. Gonzalez, "Study of molten salt corrosion of HK-40 m alloy applying linear polarization resistance and conventional weight loss techniques," *Corrosion Science*, vol. 46, no. 11, pp. 2663–2679, 2004.

[7] J. G. Gonzalez-Rodriguez, S. Haro, A. Martinez-Villafañe, V. M. Salinas-Bravo, and J. Porcayo-Calderón, "Corrosion performance of heat resistant alloys in Na_2SO_4–V_2O_5 molten salts," *Materials Science and Engineering A*, vol. 435-436, pp. 258–265, 2006.

[8] B. P. Mohanty and D. A. Shores, "Role of chlorides in hot corrosion of a cast Fe–Cr–Ni alloy. Part I: experimental studies," *Corrosion Science*, vol. 46, no. 12, pp. 2893–2907, 2004.

[9] R. Singh, J. Swaminathan, S. Paswan, V. Rajinikanth, and I. Chattoraj, "Investigations on high temperature corrosion of wire enameling oven," *Engineering Failure Analysis*, vol. 18, no. 5, pp. 1375–1387, 2011.

[10] G. Gao, F. H. Stott, J. L. Dawson, and D. M. Farrell, "Electrochemical monitoring of high-temperature molten-salt corrosion," *Oxidation of Metals*, vol. 33, no. 1-2, pp. 79–94, 1990.

[11] T. Tzvetkoff and J. Kolchakov, "Mechanism of growth, composition and structure of oxide films formed on ferrous alloys in molten salt electrolytes—a review," *Materials Chemistry and Physics*, vol. 87, no. 1, pp. 201–211, 2004.

[12] J. A. Ellor, "Uniform," in *Corrosion Test and Standard Manual Application and Interpretation*, ASTM Manual Series, ASTM, Philadelphia, Pa, USA, 1995.

[13] U. K. Chatterjee, S. K. Bose, and S. K. Roy, *Electrochemical Techniques for Corrosion Engineering*, edited by R. Baboian, NACE Publication, Houston, Tex, USA, 1986.

[14] C. Cuevas-Arteaga, "Corrosion study of HK-40m alloy exposed to molten sulfate/vanadate mixtures using the electrochemical noise technique," *Corrosion Science*, vol. 50, no. 3, pp. 650–663, 2008.

[15] C. C. Arteaga, "Corrosion evaluation of AISI-309 exposed to 50 mol% Na_2SO_4-50 mol% V_2O_5 at high temperature applying electrochemical techniques and the weight loss method," *International Journal of Electrochemical Science*, vol. 7, no. 12, pp. 12283–12300, 2012.

[16] C. Cuevas-Arteaga, V. Escalada, and M. A. Trujillo, "Molten salt corrosion evaluation of alloy T22 applying electrochemical techniques and the conventional weight loss method," *ECS Transactions*, vol. 36, no. 1, pp. 65–82, 2011.

[17] G. W. Cunningham and A. D. S. Brasunas, "The effects of contamination by vanadium and sodium compounds on the air-corrosion of stainless steel," *Corrosion Journal*, vol. 12, no. 8, pp. 389t–405t, 1956.

[18] H. Lewis, "Corrosion by vanadium-pentoxide sodium-sulphate mixtures in laboratory tests: correlation with corrosion by oil-ash in field tests," *British Petroleum Equipment News*, vol. 7, no. 4-5, pp. 17–23, 1957.

[19] L. B. Pfeil, "Corrosion of heat-resisting alloys in the presence of fuel-oil ash," *British Petroleum Equipment News*, vol. 7, no. 4-5, pp. 54–69, 1957.

[20] ASTM Standard, "G59-97: standard test method for conducting potentiodynamic polarization resistance measurements," in *Annual Book of ASTM Standards*, vol. 3, ASTM International, 2014.

[21] W. Gao and Z. Li, *Developments in High-Temperature Corrosion and Protection of Materials*, Woodhead Publishing Limited, Cambridge, UK, 1st edition, 2008.

[22] W. Skinner, "Influence of experimental inaccuracies on corrosion rates and Tafel slopes determined from electrochemical measurements in different overpotential ranges," *British Corrosion Journal*, vol. 22, no. 3, pp. 172–175, 1987.

[23] E. Poorqasemi, O. Abootalebi, M. Peikari, and F. Haqdar, "Investigating accuracy of the Tafel extrapolation method in HCl solutions," *Corrosion Science*, vol. 51, no. 5, pp. 1043–1054, 2009.

[24] M. A. Amin, K. F. Khaled, and S. A. Fadl-Allah, "Testing validity of the Tafel extrapolation method for monitoring corrosion of cold rolled steel in HCl solutions—experimental and theoretical studies," *Corrosion Science*, vol. 52, no. 1, pp. 140–151, 2010.

[25] V. Feliu, J. A. González, and S. Feliu, "Corrosion estimates from the transient response to a potential step," *Corrosion Science*, vol. 49, no. 8, pp. 3241–3255, 2007.

[26] X. Zhang, W. He, I. Odnevall Wallinder, J. Pan, and C. Leygraf, "Determination of instantaneous corrosion rates and runoff rates of copper from naturally patinated copper during continuous rain events," *Corrosion Science*, vol. 44, no. 9, pp. 2131–2151, 2002.

[27] I. D. Raistrick, D. R. Franceschetti, and J. R. Macdonald, "Chapter 2. Theory," in *Impedance Spectroscopy: Theory, Experiment, and Applications*, E. Barsoukov and J. R. Macdonald, Eds., John Wiley & Sons, Hoboken, NJ, USA, 2nd edition, 2005.

[28] J. L. Trinstancho-Reyes, M. Sanchez-Carrillo, R. Sandoval-Jabalera et al., "Electrochemical impedance spectroscopy investigation of alloy inconel 718 in molten salts at high temperature," *International Journal of Electrochemical Science*, vol. 6, no. 2, pp. 419–431, 2011.

[29] Y. J. Tan, S. Bailey, and B. Kinsella, "An investigation of the formation and destruction of corrosion inhibitor films using electrochemical impedance spectroscopy (EIS)," *Corrosion Science*, vol. 38, no. 9, pp. 1545–1561, 1996.

[30] C. Cuevas-Arteaga, J. Uruchurtu-Chavarín, J. González, G. Izquierdo-Montalvo, J. Porcayo-Calderón, and U. Cano-Castillo, "Corrosion evaluation of Alloy 800 in sulfate/vanadate molten salts," *Corrosion*, vol. 60, no. 6, pp. 548–560, 2004.

[31] C. S. Ni, L. Y. Lu, C. L. Zeng, and Y. Niu, "Electrochemical impedance studies of the initial-stage corrosion of 310S stainless steel beneath thin film of molten $(0.62Li,0.38K)_2CO_3$ at 650°C," *Corrosion Science*, vol. 53, no. 3, pp. 1018–1024, 2011.

[32] C. L. Zeng, W. Wang, and W. T. Wu, "Electrochemical impedance models for molten salt corrosion," *Corrosion Science*, vol. 43, no. 4, pp. 787–801, 2001.

[33] E. Barsoukov and J. R. Macdonald, *Impedance Spectroscopy Theory, Experiment, and Applications*, Wiley-Interscience, 2nd edition, 2005.

[34] Q.-A. Huang, R. Hui, B. Wang, and J. Zhang, "A review of AC impedance modeling and validation in SOFC diagnosis," *Electrochimica Acta*, vol. 52, no. 28, pp. 8144–8164, 2007.

[35] D. M. Farrell, W. M. Cox, J. L. Dawson, and P. D. Bottomley, "Electrochemical interfaces in high temperature sulphidation and oxidation reaction," in *Proceedings of the UK CORROSION/NACE*, 1989.

[36] J. Pan, C. Leygraf, R. F. A. Jargelius-Pettersson, and J. Lindén, "Characterization of high-temperature oxide films on stainless steels by electrochemical-impedance spectroscopy," *Oxidation of Metals*, vol. 50, no. 5-6, pp. 431–455, 1998.

[37] J. E. G. González and J. C. Mirza-Rosca, "Study of the corrosion behavior of titanium and some of its alloys for biomedical and dental implant applications," *Journal of Electroanalytical Chemistry*, vol. 471, no. 2, pp. 109–115, 1999.

[38] E. Barsoukov and J. Ross Macdonald, *Impedance Spectroscopy Theory, Experiment, and Applications*, Wiley Interscience, 2nd edition, 2005.

[39] Y. M. Wu and R. A. Rapp, "Electrochemical impedance studies of hot corrosion of preoxidized Ni by a thin-fused Na_2SO_4 film," *Journal of the Electrochemical Society*, vol. 138, no. 9, pp. 2683–2690, 1991.

[40] N. A. Al-Mobarak, A. A. Al-Swayih, and F. A. Al-Rashoud, "Corrosion behavior of Ti-6Al-7Nb alloy in biological solution for dentistry applications," *International Journal of Electrochemical Science*, vol. 6, no. 6, pp. 2031–2042, 2011.

[41] C. H. Hsu and F. Mansfeld, "Concernng the conversion of the constant phase element parameter Y0 into a capacitance," *Corrosion*, vol. 57, no. 9, pp. 747–748, 2001.

[42] D. A. López, S. N. Simison, and S. R. de Sánchez, "The influence of steel microstructure on CO_2 corrosion. EIS studies on the inhibition efficiency of benzimidazole," *Electrochimica Acta*, vol. 48, no. 7, pp. 845–854, 2003.

[43] C. L. Zeng and J. Li, "Electrochemical impedance studies of molten $(0.9Na,0.1K)_2SO_4$-induced hot corrosion of the Ni-based superalloy M38G at 900 ∘C in air," *Electrochimica Acta*, vol. 50, no. 28, pp. 5533–5538, 2005.